Phys. Biol. **9** (2012) 016011 (12pp) doi:10.1088/1478-3975/9/1/016011

Modeling the Q-cycle mechanism of transmembrane energy conversion

Anatoly Yu Smirnov[1,2] **and Franco Nori**[1,2]

[1] Advanced Science Institute, RIKEN, Wako-shi, Saitama 351-0198, Japan
[2] Physics Department, The University of Michigan, Ann Arbor, MI 48109-1040, USA

E-mail: asmirnov@riken.jp

Received 21 June 2011
Accepted for publication 5 December 2011
Published 7 February 2012
Online at stacks.iop.org/PhysBio/9/016011

Abstract
The Q-cycle mechanism plays an important role in the conversion of the redox energy into the energy of the proton electrochemical gradient across the biomembrane. The bifurcated electron transfer reaction, which is built into this mechanism, recycles one electron, thus allowing us to translocate two protons per one electron moving to the high-potential redox chain. We study a kinetic model of the Q-cycle mechanism in an artificial system which mimics the bf complex of plants and cyanobacteria in the regime of ferredoxin-dependent cyclic electron flow. Using methods of condensed matter physics, we derive a set of master equations and describe a time sequence of electron and proton transfer reactions in the complex. We find energetic conditions when the bifurcation of the electron pathways at the positive side of the membrane occurs naturally, without any additional gates. For reasonable parameter values, we show that this system is able to translocate more than 1.8 protons, on average, per one electron, with a thermodynamic efficiency of the order of 32% or higher.

S Online supplementary data available from stacks.iop.org/PhysBio/9/016011/mmedia

List of mathematical notations

U_e	Coulomb repulsion between two electrons occupying the shuttle
U_p	proton–proton electrostatic repulsion on the shuttle Q
U_{ep}	Coulomb attraction between an electron and a proton on the shuttle
U_{LH}	electrostatic interaction between electrons on the sites L and H
ε_i	energy level of an electron located on the site i
E_Q	energy level of a proton occupying the shuttle Q
$\lambda_{ii'}$	reorganization energy for electron transfer between the sites i and i'
$\Delta_{ii'}$	electron tunneling amplitude for a transition between the sites i and i'
γ_S/γ_D	A-to-S and B-to-D electron transition rates
$f_S(\varepsilon)/f_D(\varepsilon)$	Fermi distributions of electrons in the source (S) and drain (D) reservoirs
μ_S/μ_D	electrochemical potentials of source and drain electron reservoirs
Γ_N/Γ_P	rates of proton transfer between the shuttle and N or P proton reservoirs
$F_N(E)/F_P(E)$	Fermi distributions of protons in N or P reservoirs
μ_N/μ_P	electrochemical potentials of N or P proton reservoirs
V_N/V_P	absolute values of surface potential at N or P-sides of the membrane
T	equilibrium temperature of the system

1. Introduction

The energy produced by a biological system or by an artificial device must often be converted into a more stable form [1, 2]. The thermodynamic efficiency and the quantum yield of this process are of prime importance for the overall performance of the energy transducer. This transducer consumes the energy of input particles, which move energetically downhill or just disappear in the process, and transfers this energy to another

kind of particles moving energetically uphill. Here, the quantum yield (QY) is defined as the number of particles at the output of the energy transducer divided by the number of input particles. The efficiency of such a device can be higher when the quantum yield is more than 1, i.e. when a single input particle creates many output carriers.

The generation of two or more electron–hole pairs (excitons) by a single high-energy photon [3] was observed in semiconductor nanocrystals [4]. A similar situation takes place in the bc_1 complex embedded into the inner mitochondrial membrane as well as in the related complex bf [5, 6], which mediates the electron transfer between the photosystem II (PS II) and the photosystem I (PS I) in the thylakoid membranes of plants and cyanobacteria [7]. According to the generally accepted Q-cycle mechanism [8–10], the transfer of *two* electrons from a plastoquinol molecule PQH_2 to a cytochrome f and further to plastocyanin (in bf complexes) is accompanied by an energetically uphill translocation of *four* protons from the negative (N) to the positive (P) side of the membrane, resulting in a quantum yield $QY = 2$.

We note that within the standard redox loop mechanism (see [11] and references therein), only two protons are transferred in parallel with the transfer of two electrons, implying that the quantum yield is equal to 1. Hereafter, we primarily concentrate on the bf complex as a biological counterpart of our artificial system. Despite numerous studies [12–15], the physical mechanism of the Q-cycle in bc_1 and bf complexes is not completely understood.

In this work, we analyze a simple model (see figure 1) mimicking the main features of the Q-cycle in the bf complex in the regime of ferredoxin-dependent cyclic electron flow (CEF) [16–19]. In this regime, electrons cycle between the PS I and the bf complex, which are electronically connected by a pool of ferredoxin molecules (on the N-side of the membrane) and by a pool of plastocyanin molecules on the lumenal (P) side of the membrane. We treat these two pools as a source (S) and drain (D) electron reservoirs coupled to the electron-binding sites A and B, respectively. Besides the sites A and B, the membrane-embedded central complex is comprised of sites L and H, which correspond to hemes b_L and b_H of the complex bf, respectively. The sites A and H are assumed to be electronically decoupled as well as the sites B and L. A mobile shuttle Q (an analog of a plastoquinone molecule) diffuses inside the membrane, between the sites A and H (on the P-side) and the sites B and L (on the N-side). As its biological counterpart, the shuttle has two electron sites and two proton-binding sites. At its N-position, the shuttle takes one electron from the site A and another electron from the site H and transfers these electrons to the sites B and L.

At the N-side, the shuttle also accepts up to two protons from the stromal (electrically negative) proton reservoir and donates these protons to the lumenal (electrically positive) proton reservoir at the P-side of the membrane. When the fully populated Q-molecule arrives at the P-side, one electron from the shuttle goes strictly energetically downhill, to the site B, whereas another one returns to the L–H chain to be loaded again on the shuttle. The origin of this bifurcated reaction [20], which occurs at the P-side catalytic center, remains unknown.

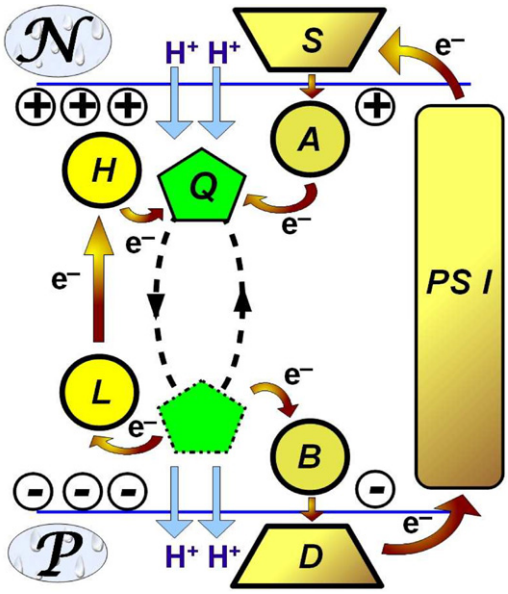

Figure 1. Simplified schematic of the Q-cycle mechanism in the regime of CEF. At the N-side of the membrane, the photosystem I (PS I) provides the source reservoir S with high-energy electrons. Via the bridge site A, the source S delivers electrons to the shuttle Q, which also accepts electrons from the site H and protons from the N-side proton reservoir. At the P-side of the membrane, the shuttle Q gives away electrons to the site L and to the drain reservoir D (via the bridge site B). In this process, two protons move to the P-side proton reservoir. From the site L, electrons return to the site H to be loaded later on the shuttle Q. The drain reservoir D transfers low-energy electrons back to the photosystem I. The surface potential V_S, which is positive at the N-side and negative at the P-side of the membrane, is shown here with circled plus ($+V_N$) and minus ($-V_P$) signs.

The site B, which accepts an electron from the quinol PQH_2 at the lumenal side of the membrane, is related to the [2Fe–2S] cluster of the Rieske iron–sulfur protein (ISP) [23]. It follows from structural data [5, 6, 23] as well as from measurements of viscosity effects on electron transfer [24] that in the bf complex, the ISP should move between the quinol and the cytochrome f, which serves as a bridge for electrons on their way to the plastocyanin pool. Two locations of the ISP, one near the cytochrome c_1 and another in the proximity of QH_2, were observed in bc_1 crystal structures [25]. These two locations are separated by a distance of the order of 25 Å [26], implying that the ISP movement is necessary to facilitate electron transfer between QH_2 and the cytochrome c_1. A similar situation takes place in the bf complex where the [2Fe–2S] cluster of ISP is about 30 Å from the cytochrome f, though no structural observations of two separated positions of ISP have been made yet [23]. It is also shown [27] that the functioning of the bf complex is not sensitive to variations of the length and flexibility of the mobile ISP hinge. There is no question that swinging of the ISP hinge is essential for electron transfer in the bf complex; however, this feature by itself cannot explain the bifurcation of electronic pathways at the P-side catalytic center. The presence or absence of an electron carrier in the right location is not enough to enforce electrons to move from one site to another. It is also necessary to provide

energetic conditions facilitating electron and proton transfer in the right direction. Here, with the immobile site B, we show that the P-side bifurcated reaction can be explained with the proper choice of energetic conditions, so that conformational changes in the Rieske protein may not play any active role in the functioning of the bf complex.

In the present model, we consider a regime of CEF. It should be noted, however, that another regime of linear electron flow (LEF) usually dominates in photosynthetic organisms [17, 21]. In the LEF regime, electrons move sequentially from water through the photosystem II, and then the complex bf, afterwards the PS I to molecules of NADPH and, finally, to the Benson–Calvin cycle. We concentrate here on the CEF regime since (i) the CEF regime is very important for maintaining the right proportion of NADPH and ATP molecules in the thylakoid membranes [16, 19], (ii) CEF prevails over LEF in some systems (e.g., in bundle sheath cells of C4 plants [16, 18]) and at some conditions (e.g., at low CO_2 concentrations and under the high intensity of light [16, 17]) and (iii) CEF is essential for turning on photoprotective mechanisms [17, 18, 22]. Including the LEF regime in our study would require a significant complication of the mathematical model.

To illustrate the basic operational principles of the Q-cycle mechanism, we explore here the physicochemical conditions wherein our artificial complex is able to translocate twice as many protons as the number of electrons transferred energetically downhill, from the source S to the drain D. Protons are translocated energetically uphill, from the N- to P-side of the membrane. We aim at the explanation of the Q-cycle operation in this artificial complex. We examine a sequence of events and combinations of parameters allowing the efficient performance of the Q-cycle scheme. The functional principles of the Q-cycle in artificial systems can provide a better understanding of the Q-cycle mechanism in natural bc_1 and bf complexes.

2. Model and methods

2.1. Components and states

To simplify the problem, we divide the whole system of six electron- and two proton-binding sites into four weakly interacting subsystems: (i) the LH-subsystem consisting of L and H sites (with energies ε_L and ε_H, respectively); (ii) the shuttle Q having two electron sites 1_e and 2_e (with energies $\varepsilon_1 = \varepsilon_2 = \varepsilon_Q$) and two proton sites 1_p and 2_p (with energies $E_1 = E_2 = E_Q$), (iii) the site A (with energy ε_A) and (iv) the site B (with energy ε_B).

The LH-subsystem is characterized by four microscopic states starting with the empty (vacuum) state, $|1\rangle_{LH} = |0_L 0_H\rangle$, and ending with the doubly occupied system: $|4\rangle_{LH} = |1_L 1_H\rangle$. The electron and proton populations of the shuttle are described by 16 states, where $|1\rangle_Q = |0_{1e} 0_{2e} 0_{1p} 0_{2p}\rangle$ is the vacuum state and $|16\rangle_Q = |1_{1e} 1_{2e} 1_{1p} 1_{2p}\rangle$ is the state of the completely loaded shuttle. Here, we use the notation 0_α (1_α) for an empty (occupied) site α, where $\alpha = 1_e, 2_e$ for the electron sites on the shuttle and $\alpha = 1_p, 2_p$ for the proton sites. The average populations of the sites A and B are denoted by $\langle n_A \rangle$ and $\langle n_B \rangle$, respectively. Here $\langle \cdots \rangle = \langle \langle \Psi_0 | \ldots | \Psi_0 \rangle \rangle_T$ means double-averaging over an initial wavefunction Ψ_0 and over a thermal distribution $\langle \cdots \rangle$ of reservoirs and environment characterized by the common temperature T.

We take into account strong Coulomb interactions between sites from the same subsystem. A Coulomb repulsion between electrons located on the sites L and H (LH-subsystem) is characterized by the energy u_{LH}, whereas for the electrons and protons on the shuttle (Q-subsystem) we introduce the following parameters: U_e (Coulomb repulsion between two electrons occupying the shuttle sites 1_e and 2_e); U_p (electrostatic repulsion between two protons located on the sites 1_p and 2_p); and $U_{ij} = U_{ep}$ (electron–proton Coulomb attraction on the shuttle). Here the indices $i = 1, 2$ and $j = 1, 2$ run over the electron- and proton-binding sites of the shuttle, respectively.

2.2. Electron and proton transitions

Electrons can tunnel between the L and H sites as well as between sites belonging to different subsystems. These tunnelings are described by relatively small tunneling amplitudes: Δ_{LH} (L–H tunneling); $\Delta_{HQ}(x)$ (tunneling between the H site and the $1_e, 2_e$ sites; $\Delta_{LQ}(x)$ (for electron transitions between the $1_e, 2_e$ and L sites. The amplitudes $\Delta_{AQ}(x)$ and $\Delta_{BQ}(x)$ describe the tunneling between the bridge sites A, B and the electron sites $1_e, 2_e$ on the shuttle. The amplitudes Δ_{AQ}, Δ_{HQ} and Δ_{BQ}, Δ_{LQ} depend on the position x of the mobile molecule Q. The proton rates $\Gamma_N(x)$ (for transitions between the sites $1_p, 2_p$ and the N-side proton reservoir) and $\Gamma_P(x)$ (for transitions between the proton sites on the shuttle and the P-reservoir) are also functions of x.

2.3. Brownian motion of the shuttle

It is known [23, 28] that the quinone exchange cavity in the bf complex contains about six plastoquinones for each cytochrome f. This cavity is quite spacious (30 Å × 15 Å × 25 Å). An average linear size of a plastoquinone molecule is of the order of 7 Å [29]. This means that collisions between quinone molecules can occasionally take place. The value of the quinone diffusion coefficient $\mathcal{D}$ used in our calculations is close to experimental values measured in the system having many quinone molecules. Thus, quinone–quinone collisions are implicitly included in the diffusion coefficient $\mathcal{D}$. Here, we restrict ourselves to the case of a single shuttle diffusing inside the lipid membrane. The mechanical motion of the shuttle is presumably the slowest process in the system. Thus, many shuttles should accelerate the translocation of electrons and protons across the system. For example, in the case of two shuttles, one of them (P-shuttle, which is fully loaded with two electrons and two protons) can be near the P-side catalytic center (sites L and B), whereas another empty N-shuttle can simultaneously bind to the N-side center (sites A and H). Thus, an electron unloaded from the P-shuttle to the L–H chain will be almost immediately transferred to the N-shuttle, which will take another electron from the site A and two protons from the P-side of the membrane. This fully loaded shuttle can now

move to the P-side of the membrane. Here, there is no time delay related to the slow mechanical return of the unloaded P-shuttle to the N-side catalytic center. It means that, with two translocators, the proton pumping process can be accelerated two times or so.

The time evolution of $x(t)$ is determined by an overdamped Langevin equation, with terms describing walls of the membrane and a potential barrier (see equation (A.13) in the appendix), which impedes the charged shuttle to cross the intermembrane space [30, 31]. The walls of the membrane are located at $x = -x_0$ (N-side) and at $x = x_0$ (P-side), so that the width of the membrane is equal to $2x_0$. Note that a quinone molecule playing the role of shuttle in natural systems has a long isoprenoid chain [23]. Because of this lipophilic tail, a quinone is not able to move in a water environment outside the lipid bilayer membrane.

2.4. Equations and simulation procedure

Using the formalism outlined in [30–33] and based on Marcus transition rates [34], we derive and numerically solve a set of master equations (see the appendix and supporting information available at stacks.iop.org/PhysBio/9/016011/mmedia) for an electron distribution $\langle R_M \rangle$ over states of the LH-subsystem coupled to a system of equations for the probabilities $\langle \rho_\mu \rangle$ to find the Q-subsystem in the state $|\mu\rangle$. These equations are complemented by equations for the populations $\langle n_{\rm A} \rangle$and $\langle n_{\rm B} \rangle$ of the A- and B-sites, respectively, and by an overdamped Langevin equation for the shuttle position $x(t)$.

It should be noted that electron and proton transitions are usually much faster than the mechanical motion of the shuttle across the lipid membrane. Therefore, we can average the equations for the electron and proton variables over the equilibrium states of the electron and proton reservoirs, as well as over fluctuations of protein environment at the given point $x(t)$. The diffusion of the shuttle itself is described by a stochastic equation (see equation (A.13) in the appendix). The motion of the lipophilic shuttle is restricted by the walls of the lipid membrane and by the barrier, which does not allow for the charged translocator to cross the membrane.

As a result of simulations, we obtain a single stochastic trajectory $x(t)$ of the shuttle complemented by time-dependent populations of electron- and proton-binding sites. At each moment of time t, these populations are averaged over electron and proton reservoirs. We emphasize, however, that we take into account not only averaged populations, but also correlations between strongly interacting electron and proton sites. To do this, we introduce 4 states for the LH-subsystem, having just two electron-binding sites, and 16 basis states for two electron- and two proton-binding sites on the shuttle Q (see the appendix and the supporting information section available at stacks.iop.org/PhysBio/9/016011/mmedia) with the corresponding distributions $\langle R_M \rangle$ and $\langle \rho_\mu \rangle$. For the Q-subsystem (the shuttle), the distributions $\langle \rho_2 \rangle$, $\langle \rho_3 \rangle$ and $\langle \rho_5 \rangle$, $\langle \rho_6 \rangle$ describe the populations of two electron and two proton sites on the shuttle, respectively, whereas the functions $\langle \rho_4 \rangle$ and $\langle \rho_7 \rangle$ define correlations between two electron or between two protons simultaneously occupying the shuttle. Other distributions, $\langle \rho_8 \rangle, \ldots, \langle \rho_{16} \rangle$, describe electron–proton correlations on the shuttle (see equation (15) of the supporting information available at stacks.iop.org/PhysBio/9/016011/mmedia).

To obtain the numbers of transferred electrons and protons, which can be measured in experiments (see, e.g., [35, 36]), we take the time averaging of our output functions over a long stochastic trajectory including numerous back-and-forth trips of the shuttle. Numerically, we also average our results over many realizations of the random function $x(t)$.

2.5. Potentials

It is known [7] that charged ions, such as Mg^{2+} and Cl^-, can easily cross a thylakoid membrane, which results in the equilibration of electrical potentials on both sides of a membrane. Therefore, the difference between the proton electrochemical potential $\mu_{\rm P}$ of the P-side and the potential $\mu_{\rm N}$ of the N-side of the membrane [7] is mainly determined by the proton concentration gradient ΔpH :

$$\mu_{\rm P} - \mu_{\rm N} \simeq -\Delta p{\rm H} \times (T/T_{\rm R}) \times 60\,{\rm meV}, \tag{1}$$

where T is the temperature of the reservoirs and $T_{\rm R} = 298$ K is the room temperature. It should be noted, however, that a surface potential $V_S(x)$, which is positive on the N-side, $V_S(-x_0) = +V_{\rm N}$, and negative, $V_S(x_0) = -V_{\rm P}$, on the P-side of the membrane (see circled plus and minus signs in figure 1 for the potentials $+V_{\rm N}$ and $-V_{\rm P}$, respectively), was calculated for the *bf* complex of *M. laminosus* [23] with $V_{\rm N} = 4.6$ T and $V_{\rm P} = 5.4$ T (the Boltzmann constant $k_B = 1$). This model assumes that there is a similar transmembrane potential (see figure 1),

$$V_S(x) = -\frac{x - x_0}{2x_0} V_{\rm N} - \frac{x + x_0}{2x_0} V_{\rm P}, \tag{2}$$

with $V_{\rm N} \simeq 120$ meV and $V_{\rm P} \simeq 140$ meV, which correspond to the above-mentioned values of $V_{\rm N}$ and $V_{\rm P}$ at room temperature. All energies are measured in meV. In the presence of the surface potential, the energy levels of electrons and protons on the shuttle are shifted from their initial values $\varepsilon_{\rm Q0}$ and $E_{\rm Q0}$ depending on the shuttle's position x:

$$\begin{aligned} \varepsilon_{\rm Q}(x) &= \varepsilon_{\rm Q0} - V_S(x), \\ E_{\rm Q}(x) &= E_{\rm Q0} + V_S(x), \end{aligned} \tag{3}$$

with $\varepsilon_{\rm QN} = \varepsilon_{\rm Q0} - V_{\rm N}$, $\varepsilon_{\rm QP} = \varepsilon_{\rm Q0} + V_{\rm P}$ and $E_{\rm QN} = E_{\rm Q0} + V_{\rm N}$, $E_{\rm QP} = E_{\rm Q0} - V_{\rm P}$. Correspondingly, the energy levels of the electron sites A and H, located near the N-side, are shifted down from their initial values: $\varepsilon_{\rm A} = \varepsilon_{\rm A0} - V_{\rm N}$, $\varepsilon_{\rm H} = \varepsilon_{\rm H0} - V_{\rm N}$, whereas the energies of the sites B and L, located near the P-side, are shifted up: $\varepsilon_{\rm B} = \varepsilon_{\rm B0} + V_{\rm P}$, $\varepsilon_{\rm L} = \varepsilon_{\rm L0} + V_{\rm P}$.

3. 'Passenger' scenario of the Q-cycle

Instead of searching over a multidimensional space of system parameters, we consider a reasonable sequence of events, which provides an optimal performance of the energy transducer. In particular, we analyze a scenario where an electron transferred from the high-energy source reservoir S along the chain: S → A → Q → B → D to the drain D performs the main energetic function in the transfer of two

protons from the N- to the P-side of the membrane. Another electron traveling on the shuttle and recycled by the LH-system along the chain H → Q → L → H plays a more passive role of a passenger, which is necessary to compensate a shuttle charge.

According to the Marcus formula [34] (see also the appendix)

$$\kappa_{ii'} = |\Delta_{ii'}|^2 \sqrt{\frac{\pi}{\lambda_{ii'} T}}\ \exp\left[-\frac{(\varepsilon_i - \varepsilon_{i'} - \lambda_{ii'})^2}{4\lambda_{ii'} T}\right], \qquad (4)$$

the rate $\kappa_{ii'}$ for an electron transition from the site i, with an energy ε_i, to the site i', with an energy $\varepsilon_{i'}$, has a maximum at $\varepsilon_i = \varepsilon_{i'} + \lambda_{ii'}$. Here $\Delta_{ii'}$ is the tunneling amplitude between the sites i and i', $\lambda_{ii'}$ is the corresponding reorganization energy, which is due to electron coupling to an environment with temperature T. The shuttle can accept protons from the N-reservoir provided that the electrochemical potential of the N-side, μ_N, is higher than the proton energy level on the shuttle. Protons move from the shuttle Q to the P-side reservoir if the energy of the Q-proton exceeds the P-side potential μ_P.

3.1. Sequence of events and energy relations

We start with a situation when the empty shuttle (quinone) is near the N-side catalytic center, $x = -x_0$, and the LH-system (analog of cytochrome *b* in the *bf* complex) is preloaded with one electron located presumably at the site H, which has a lower energy than the site L: $\varepsilon_L > \varepsilon_H$. The site A is also occupied with an electron taken from the electron source S. We have the following sequence of electron (e) and proton (p) transfer from and to the shuttle located near the N-side of the membrane:

(a) e : H → Q, $\varepsilon_H = \varepsilon_{QN} + \lambda_{HQ}$.
(b) e : A → Q, $\varepsilon_A = \varepsilon_{QN} + U_e + \lambda_{AQ}$.
(c) p : N → Q, $\mu_N > E_{QN} - 2U_{ep}$.
(d) p : N → Q, $\mu_N > E_{QN} - 2U_{ep} + U_p$.

Here we have written relations between energy levels of electrons and protons which make possible these transfers.

The shuttle loaded with two electrons and two protons travels to the P-side of the membrane, where the following sequence of electron and proton transitions occurs:

(e) e : Q → B, $\varepsilon_{QP} + U_e - 2U_{ep} = \varepsilon_B + \lambda_{BQ}$.
(f) p : Q → P, $E_{QP} - U_{ep} + U_p > \mu_P$.
(g) p : Q → P, $E_{QP} - U_{ep} > \mu_P$.
(h) e : Q → L, $\varepsilon_{QP} = \varepsilon_L + \lambda_{LQ}$.

Finally, an electron tunnels from the L to the H site:

(i) e : L → H, $\varepsilon_L = \varepsilon_H + \lambda_{LH}$.

The empty shuttle diffuses to the N-side of the membrane and the process repeats. We expect that two protons will be translocated from the N-side to the P-side of the membrane per one electron transferred from the source to the drain electron reservoir with a quantum yield QY = 2.

Here we assume that, as in the case of the quinone molecule Q [37], the shuttle populated with one electron (after step a) does not bind a proton but accepts another electron (step b). The doubly reduced quinol is known to have a much stronger ability for binding two protons (see steps c and d). At the P-side of the membrane, the process presumably evolves in the opposite direction when the transfer of one electron from Q to the site B is accompanied by the unloading of two protons. In the absence of an attraction to two positive charges, the energy of the electron remaining on the shuttle goes up, thus allowing its tunneling to the L-site.

Here, an electron recycled by the LH-system plays a passive role of a shuttle's 'passenger' since its transitions to and from the Q-molecule are not immediately accompanied by a proton transfer. Transitions of another electron, which is loaded to the shuttle from the source S (via the site A) and unloaded to the drain D (via the site B), are more closely coupled to the energetically uphill proton translocation.

It follows from relations (a), (h) and (i) in this section that the recycling of one electron by the L–H chain, H → Q → L → H, which lies at the heart of the Q-cycle, takes place if the difference of surface potentials,

$$\Delta V = V_S(-x_0) - V_S(x_0) = V_N + V_P, \qquad (5)$$

is of the order of the total reorganization energy along the recycling path:

$$\Delta V = \lambda_{HQ} + \lambda_{LQ} + \lambda_{LH}. \qquad (6)$$

We see from relations (d) and (g) in this section that the energetically uphill proton transfer from the N- to the P-side of the membrane is possible if the original energy of the proton on the shuttle, E_{Q0}, obeys the following inequality:

$$\mu_N + 2U_{ep} - U_p - V_N > E_{Q0} > \mu_P + U_{ep} + V_P, \qquad (7)$$

which can be true only for a sufficiently strong attraction potential, U_{ep}, between electrons and protons on the shuttle,

$$U_{ep} > \mu_P - \mu_N + \Delta V + U_p. \qquad (8)$$

Relations (a), (b), (e), (h) and (i) in this section allow us to estimate the original energies of the electron-binding sites counted, e.g., from the level ε_{B0}:

$$\begin{aligned} \varepsilon_{A0} &= \varepsilon_{B0} + 2U_{ep} + \lambda_{AQ} + \lambda_{BQ}, \\ \varepsilon_{H0} &= \varepsilon_{B0} + 2U_{ep} - U_e + \lambda_{BQ} + \lambda_{HQ}, \\ \varepsilon_{Q0} &= \varepsilon_{B0} + 2U_{ep} - U_e + \lambda_{BQ}, \\ \varepsilon_{L0} &= \varepsilon_{B0} + 2U_{ep} - U_e + \lambda_{BQ} - \lambda_{LQ}. \end{aligned} \qquad (9)$$

We assume that the potentials of the electron source, μ_S, and the electron drain, μ_D, are of the order of the energies of the A and B sites, respectively: $\mu_S = \varepsilon_A$, $\mu_D = \varepsilon_B$. Taking into account equations (9), we obtain a relation for the source–drain energy drop,

$$\mu_S - \mu_D \geqslant 2U_{ep} + \lambda_{AQ} + \lambda_{BQ} - \Delta V. \qquad (10)$$

With equations (6) and (8), we obtain the following requirement for the energy difference between the source and drain electron reservoirs:

$$\mu_S - \mu_D > 2(\mu_P - \mu_N) + 2U_p + \lambda_{tot}, \qquad (11)$$

where the combined reorganization energy,

$$\lambda_{tot} = \lambda_{AQ} + \lambda_{BQ} + \lambda_{HQ} + \lambda_{LQ} + \lambda_{LH}, \qquad (12)$$

accumulates all losses along both electron transport chains: A → Q → B and H → Q → L → H.

3.2. Thermodynamic efficiency and quantum yield

The thermodynamic efficiency η of proton translocation can be defined as

$$\eta = \frac{\mu_P - \mu_N}{\mu_S - \mu_D} \times \frac{N_P}{n_D}, \tag{13}$$

where N_P is the number of protons translocated from the N- to the P-side of the membrane and n_D is the number of electrons transferred from the source S to the electron drain D. The efficiency η is proportional to the quantum yield

$$\mathrm{QY} = \frac{N_P}{n_D}. \tag{14}$$

It follows from equation (11) that, within the 'passenger' scenario, the efficiency η of the electron-to-proton energy conversion can be estimated as

$$\eta = \frac{\mu_P - \mu_N}{2\,(\mu_P - \mu_N) + 2\,U_p + \lambda_{tot}} \times \mathrm{QY}. \tag{15}$$

This means that for a high electrochemical proton gradient, $\mu_P - \mu_N \gg U_p + 0.5\,\lambda_{tot}$, the efficiency η has the maximum: $\eta = \mathrm{QY}/2$. Thus, in the ideal case, when $\mathrm{QY} = 2$, the thermodynamic efficiency can reach the perfect mark, $\eta = 1$, when almost all electron energy is converted to the transmembrane proton-motive force.

4. Results and discussions

4.1. Parameters

In the model presented here, an electron transport chain begins at the source reservoir S, corresponding to a pool of ferredoxin (Fd) molecules, which carry electrons from the photosystem I to the *bf* complex (see figure 1). The electron drain D is related to the high-potential chain of the *bf* complex comprised of the ISP, cytochrome *f* and soluble plastocyanin (PC) molecules. Taking into account a redox potential of ferredoxin, $E_m = -0.41$ V, and the fact that a redox potential of the ISP/*f*/PC chain, E_m, is in the range from 0.3 to 0.45 V [23], we estimate that the total energy drop between the source and the drain, $\mu_S - \mu_D$, takes values from 710 up to 860 meV.

We also assume that, as for the *bf* complex [23], the surface voltage gradient, $\Delta V = V_N + V_P = 260$ meV, has been applied to the membrane, with a positive potential, $V_S(-x_0) = V_N = 120$ meV, at the N-side and a negative potential, $V_S(x_0) = -V_P = -140$ meV, at the P-side of the membrane.

The system reaches its optimal performance when $U_{ep} = 610$ meV. Hereafter, we assume that $U_e = U_{ep}/2$, $U_p = U_{ep}/8$, $U_{LH} = 240$ meV. We use the following values for the electron transfer rates, $\gamma_S = \gamma_D = 0.1\,\mu$eV, proton transition rates, $\Gamma_N = \Gamma_P = 2\,\mu$eV, and for peak values of the electron tunneling amplitudes, $\Delta_{AQ}(-x_0) = \Delta_{DQ}(x_0) = 0.1$ meV, $\Delta_{HQ}(-x_0) = \Delta_{LQ}(x_0) = 0.06$ meV. The coefficients γ_S and γ_D determine the rates of the electron transfer between the site A and the source S, and between the site B and the drain D, respectively (see the definitions of γ_S and γ_D in the appendix and in subsection I.C of the supporting information available at stacks.iop.org/PhysBio/9/016011/mmedia). The rates Γ_N and Γ_P, describing proton transitions between the N-side reservoir and the shuttle as well as between the shuttle and the P-side of the membrane, respectively, are defined in the appendix and in subsection I.E of the supporting information available at stacks.iop.org/PhysBio/9/016011/mmedia. We note that, for $\hbar = 1$, we can measure electron and proton rates in units of energy, with the rate $1\,\mu\mathrm{eV}/\hbar = 1.52\ \mathrm{ns}^{-1}$, corresponding to a transfer of 1.52 particle (on average) per nanosecond. The Brownian motion of the shuttle is governed by the Langevin equation (A.13) described in the appendix. For the diffusion coefficient of the shuttle, $\mathcal{D} = T/\zeta$, we use the value $\mathcal{D} \simeq 8 \times 10^{-12}\ \mathrm{m^2\ s^{-1}}$, which is close to experimental data for plastoquinone molecules in a lipid membrane [29]. Here ζ is the drag coefficient of the shuttle. We assume that the Boltzmann constant $k_B = 1$. We also assume that the reorganization energies, corresponding to H-Q and L-Q transitions, are equal, $\lambda_{HQ} = \lambda_{LQ}$, and the same relation is true for the A-Q and B-Q transitions: $\lambda_{AQ} = \lambda_{BQ}$.

We note that the values of the electron energy drop, $\mu_S - \mu_D$, as well as values of the transmembrane proton gradient, $\mu_P - \mu_N$, are taken from experiments (see [7, 23]). The used value of the diffusion coefficient $\mathcal{D}$ is also closely related to experimental data [29]. For calculations of surface potentials V_N and V_P, we refer to section 2.5 of [23]. For other parameters, we use reasonable values, which result in the optimal performance of the proposed Q-cycle mechanism.

4.2. Time evolution of a proton translocation process

A proton translocation process is shown in figure 2, where we plot the time dependence of the total electron, $n_Q = \langle n_1\rangle + \langle n_2\rangle$, and proton, $N_Q = \langle N_1\rangle + \langle N_2\rangle$, populations of the shuttle (figure 2(*b*)), together with the time-evolving position of the shuttle $x(t)$ (figure 2(*a*)). Here, we also show (see figure 2(*c*)) the populations of the L-site, $\langle n_L\rangle$, and H-site, $\langle n_H\rangle$, the average number of electrons $\langle n_D\rangle$ transferred from the source to the drain, as well as the average number of protons $\langle N_P\rangle$ translocated from the N-side to the P-side proton reservoir. The brackets $\langle\cdots\rangle$ are dropped in figures 2(*c*) and (*d*) for the notations of the populations, and throughout the paper, except in the appendix.

For the sake of illustration, in figure 2(*a*), we present results of simulations of a single stochastic trajectory of the shuttle. Here, the output parameters, such as numbers of electrons, n_D, and protons, N_P, have been averaged over distributions of electrons and protons in the corresponding reservoirs as well as over fluctuations of a protein environment. However, to obtain their values, which can be measured in experiments, it is necessary to average the results over many stochastic trajectories, as is done in figures 3 and 4. This procedure corresponds to the situation where an experiment is repeated many times with the same macroscopic conditions or with a set of similar samples. As a result of this averaging, we can obtain non-integer numbers of electrons and protons translocated through the system as was observed in experiments [35, 36].

Data for figure 2 are calculated at room temperature, $T = T_R = 298$ K, and at the following values of the

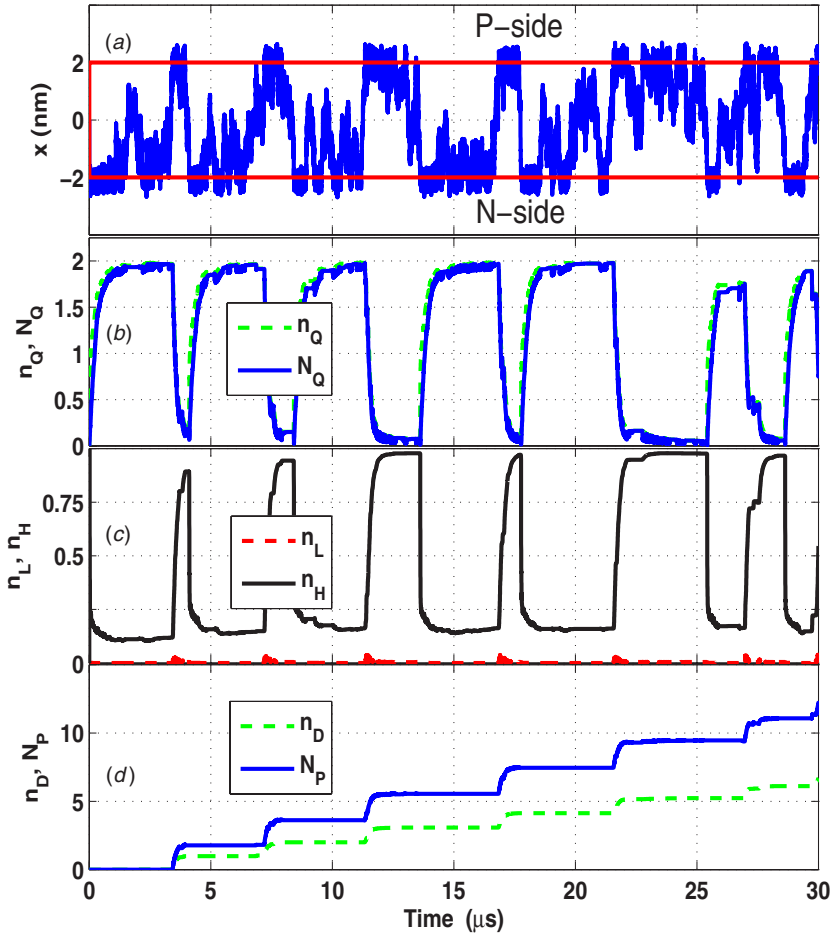

Figure 2. (*a*) Time evolution of the position $x(t)$ of the shuttle diffusing between the membrane walls located at $x = \pm 2$ nm; (*b*)–(*d*) a sequence of electron and proton transfer reactions at the following set of parameters: $\mu_S - \mu_D = 850$, $\mu_P - \mu_N = 150$, $U_{ep} = 610$ meV and $\Delta V = 260$ meV. Here we present results of simulations of a single stochastic trajectory. The total proton population N_Q of the shuttle (blue continuous line in (*b*)) almost coincides with the electron population n_Q marked by the dashed green line. The bifurcated electron transfer reaction takes place at the P-side of the membrane (at $x = 2$ nm) where one electron moves from Q to the site B and the drain D (see, e.g., a step down for n_Q in (*b*) and a step up for n_D in (*d*) at the moment $t \sim 3\mu$s). At almost the same time, another electron moves to the site L (see a barely visible dashed red line in (*c*)) and rapidly proceeds to the site H (blue continuous spike in (*c*)). Two protons are unloaded from the shuttle to the P-side of the membrane as follows from the step for N_P (blue continuous curve in (*d*)). It can be seen from (*d*) that the number of protons N_P translocated to the P-side (blue continuous line) is nearly twice as large as the number of electrons n_D moved to the drain (dashed green line).

reorganization energies: $\lambda_{LQ} = \lambda_{HQ} = 100$, $\lambda_{LH} = 250$ and $\lambda_{AQ} = \lambda_{BQ} = 100$ meV. We assume that $U_{ep} = 610$, $\Delta V = 260$, $\mu_S - \mu_D = 850$ and $\mu_P - \mu_N = 150$ meV. The proton electrochemical gradient corresponds to the value $\Delta pH = -2.5$ at room temperature. We note that these parameters are closely related to the values (see equations (6) and (11)) required for the optimal performance of the mechanism.

It can be seen from figure 2 that during 30 μs, the shuttle performs about eight trips from the N-side ($x = -x_0$) to the P-side ($x = x_0 = 2$ nm) of the membrane and back, translocating in the process about 7 electrons ($n_D = 6.7$) and 12 protons ($N_P = 12.2$), with quantum yield QY $\simeq 1.8$, and thermodynamic efficiency $\eta = 32\%$. The walls of the lipid membrane are not rigid (see, e.g., the potential $U_c(x)$ describing these walls in section 2.3 of [31]). Therefore, from time to time the shuttle can cross membrane borders located at $x = \pm 2$nm.

At the N-side (see figure 2(*b*)), the shuttle accepts an electron from the initially populated site H and another electron from the source S (via site A) as well as two protons from the N-side proton reservoir. We note (see figure 2(*c*)) that site H is not completely depopulated. This means that there are events when both electrons occupying the shuttle arrive from the site A and the source S, shorting out the Q-cycle pathway. This leakage process increases the number of electrons transferred from the source to the drain (with the same number of protons), thus decreasing the quantum yield QY.

Here we do not impose any additional restrictions, except a proper choice of energy levels, which are close to values given by equations (7), (9) and (11), with $\mu_S = 410$, $\varepsilon_A = 465$, $\varepsilon_H = 220$ and $\varepsilon_{QN} = 160$, $E_{QN} = 982$, at the N-side catalytic center (all energies are measured in meV). For the P-side center, we use the following energies: $\varepsilon_{QP} = 420$, $E_{QP} = 722$, for electrons and protons on the shuttle, $\varepsilon_B = -495$, $\mu_D = -440$, for the high-potential redox chain,

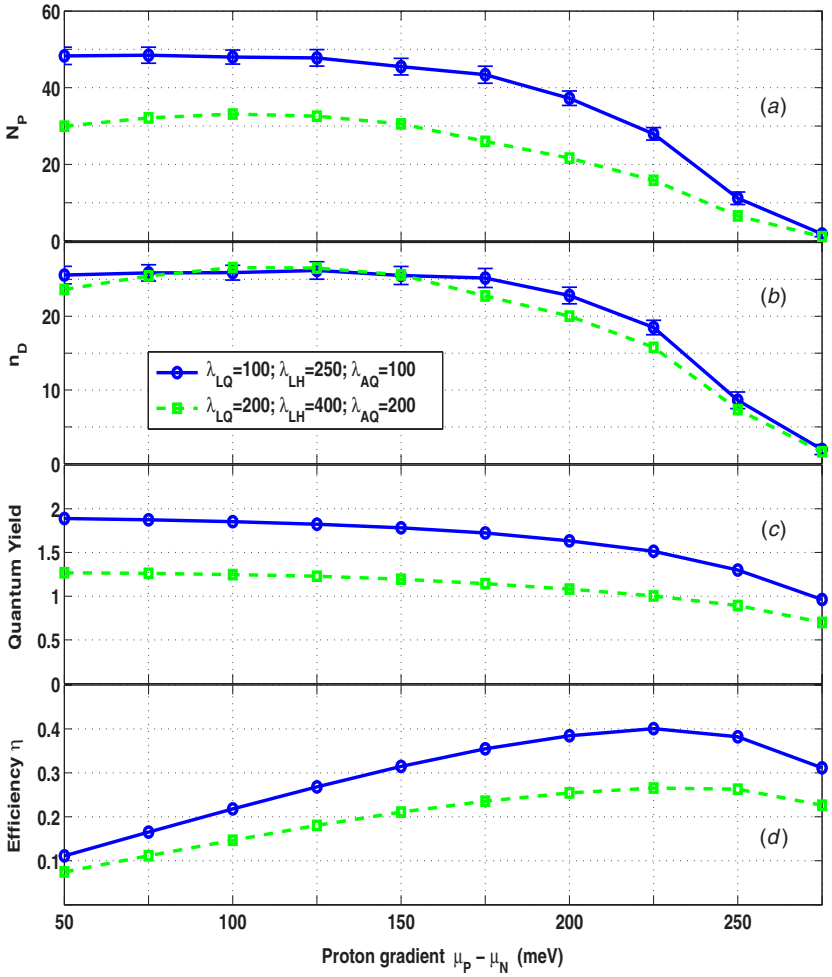

Figure 3. (*a*) Number of protons N_P transferred to the P-side of the membrane; (*b*) number of electrons n_D moved to the drain; (*c*) their ratio (quantum yield QY); (*d*) the thermodynamic efficiency η as functions of the transmembrane proton gradient $\mu_P - \mu_N$ (measured in meV) for different couplings to the environment (in meV): weaker couplings (i) $\lambda_{LQ} = 100$, $\lambda_{LH} = 250$, $\lambda_{AQ} = 100$ (blue continuous curves) and stronger couplings (ii) $\lambda_{LQ} = 200$, $\lambda_{LH} = 400$, $\lambda_{AQ} = 200$ (green dashed curves). Other parameters are the same as in figure 2. The data are averaged over ten stochastic realizations. Each realization lasts for 100 μs. These graphs demonstrate the ability of the system to translocate protons against the gradient up to 200 meV with an efficiency η up to 40%. Error bars are attached to N_P and n_D for case (i) of weak coupling to the environment.

and $\varepsilon_L = 360$ meV for the recycling pathway. This choice of energy levels makes the H-to-Q electron transition (at the N-side) much easier than the A-to-Q electron transfer, since $\varepsilon_H - \varepsilon_{QN} \leqslant \lambda_{HQ}$, whereas $\varepsilon_A - \varepsilon_{QN} \gg \lambda_{AQ}$. Moreover, the S-to-A electron transition is also hampered since the energy level of the A-site, ε_A, is higher than the potential of the source, μ_S.

On arrival at the P-side of the membrane, the shuttle donates an electron to the B-site and, finally, to the drain D. Two protons move to the P-side proton reservoir (figures 2(*b*) and (*d*)). It is evident from figure 2(*c*) that another electron from the shuttle Q goes to the L-site (see the small spike at the bottom of figure 2(*c*)). This electron is rapidly transferred to the H-site and the empty shuttle returns to the N-side.

Figures 2(*b*)–(*d*) illustrate the bifurcated reaction which occurs at the P-side. Here, one electron from the shuttle Q goes to the high-potential (and low-energy) chain, Q → B → D, while another electron (a passenger) returns to the LH-system for recycling (along the pathway Q → L → H). No additional gate mechanisms are required for this reaction. An escape of the first electron from Q to B, followed by the transition of two protons to the P-reservoir, increases the energy of the remaining electron to the level $\varepsilon_{QP} = 420$ meV, which is of order of the L-site energy, $\varepsilon_L = 360$ meV, but is much higher than the energy of the B-site, $\varepsilon_B = -495$ meV. Furthermore, the site B can still be partially occupied with an electron, which previously escaped from the shuttle. These two factors strongly suppress the leakage of the second electron from the shuttle to the high-potential chain. We note that leakage processes both at the N- and P-side centers are manifested in the fact that the experimentally measured ratio [36] between the number of protons translocated from N- to P-side of the membrane and the number of electrons transferred from PQH_2 to plastocyanin (in *bf* complexes) never reaches the perfect mark, QY = 2. The effects of short-circuiting in bc_1 complexes have also been observed in [12].

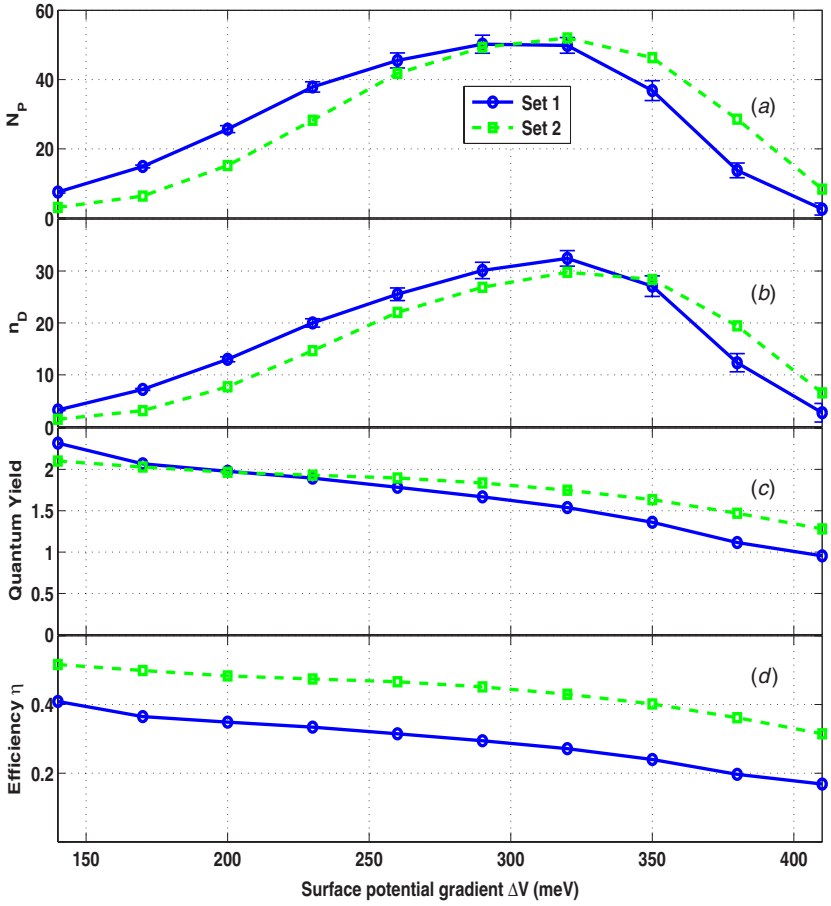

Figure 4. Dependence of the output indicators of the system: the number of protons translocated to the P-side, N_P (*a*); the number of electrons moved to the drain, n_D (*b*); the quantum yield QY(*c*); and the efficiency η (*d*), on the surface potential gradient $\Delta V = V_N + V_P$ across the membrane. Two kinds of curves correspond to two sets of energy values: (1) $\mu_S - \mu_D = 850$, $\mu_P - \mu_N = 150$, $U_{ep} = 610$ meV (blue continuous curves) and (2) $\mu_S - \mu_D = 1220$, $\mu_P - \mu_N = 300$, $U_{ep} = 800$ meV (green dashed curves) and for $\lambda_{LQ} = 100$, $\lambda_{LH} = 250$, $\lambda_{AQ} = 100$ meV. It can be seen that the system is operational in the range of the surface potentials from $\Delta V = 230$ up to $\Delta V = 350$ meV. In agreement with equation (15), the complex works more efficiently (with $\eta \sim 50\%$ and QY ~ 2) for the second set of parameters where both electron and proton gradients are higher. Here, every point is the result of averaging over ten realizations of $x(t)$, each lasting for 100 μs. For the set of parameters (1), the numbers of protons N_P and electrons n_D are plotted with error bars (standard deviations).

4.3. Effects of the proton electrochemical gradient

In figure 3, we show the numbers of protons, N_P, and electrons, n_D, transferred across the membrane, as well as the quantum yield, QY, and the power-conversion efficiency, η, as functions of the proton electrochemical gradient, $\mu_P - \mu_N$ (measured in meV). The graphs are plotted for two sets of reorganization energies: (i) $\lambda_{LQ} = \lambda_{HQ} = 100$, $\lambda_{LH} = 250$, $\lambda_{AQ} = \lambda_{BQ} = 100$ meV (blue curves); (ii) $\lambda_{LQ} = \lambda_{HQ} = 200$, $\lambda_{LH} = 400$, $\lambda_{AQ} = \lambda_{BQ} = 200$ meV (green dashed curves). Other parameters, such as $U_{ep} = 610$, $\mu_S - \mu_D = 850$, $\Delta V = 260$ (in meV), are the same as in figure 2.

We numerically calculate the output of the system (N_P, n_D, etc) at the end of the stochastic trajectory $x(t)$ (with the duration $t = 100$ μs) and average results over ten trajectories. For each value of the shuttle's position $x(t)$, we solve a set of master equations (A.1), (A.5) and (A.11), which have been averaged over electron and proton reservoirs as well as over fluctuations of the environment coupled to the electronic degrees of freedom. This can be done since the electron and proton transitions are much faster than the mechanical motion of the shuttle. In figures 3(*a*) and (*b*), for one set of parameters, we show the standard deviations, such as $\sigma_P = \sqrt{\langle N_P^2 \rangle - \langle N_P \rangle^2}$, for the numbers of protons N_P and electrons n_D. The error bars demonstrate that variations of the output parameters of the system from one stochastic trajectory $x(t)$ to another are quite small.

It follows from figure 3 that more protons, $N_P \simeq 45$, and electrons, $n_D \simeq 25$, are transferred across the membrane at lower proton gradients, $\mu_P - \mu_N \leqslant 150$ meV with a higher quantum yield, QY $\geqslant 1.8$. However, the thermodynamic efficiency is higher, $\eta \simeq 39\%$, at larger proton gradients, $\mu_N - \mu_P \simeq 200$ meV, where $N_P \sim 40$ and QY ~ 1.6. This result is in line with equation (15) which predicts an almost perfect mark for the efficiency η at very large values of the proton gradient. We note that the present model does not impose any principal limitations on the thermodynamic efficiency η. Nevertheless, for realistic parameters this

efficiency is always less than 50 %, even though the quantum yield is about 2.

The above-mentioned numbers are for set (i), with smaller values of the reorganization energies (see the blue continuous curves in figure 3). A stronger electron–environment interaction, described by set (ii) of reorganization energies, significantly reduces an energetically uphill proton flow with almost no impact on the electron current (see the green dashed curves in figure 3). In this case, the quantum yield drops to almost 1, which means that the recycling pathway (via the LH-system) is practically closed.

It is of interest that figure 3(*b*) shows a slowing of electron flow through the *bf* complex when the proton gradient increases. This regulation of electron flow is of biological importance for a photoprotection of the organism against excessive light [17, 18].

4.4. Effects of the surface potential gradient

Figure 4 demonstrates the performance of the system as a function of the surface potential gradient, $\Delta V = V_N + V_P$, at a fixed difference between the N-side and P-side potentials, $V_P - V_N = 20$ meV. Here we choose two sets of system parameters. The first set (see the blue continuous curves in figure 4), with $U_{ep} = 610$, $\mu_S - \mu_D = 850$ and $\mu_P - \mu_N = 150$ meV, was considered before. The second set (green dashed curves in figure 4) is characterized by a higher electron–proton attraction potential, $U_{ep} = 800$ meV, and a higher source–drain difference, $\mu_S - \mu_D = 1220$ meV. At these parameters, the system can translocate protons against the electrochemical difference $\mu_P - \mu_N = 300$ meV, which is related to the proton concentration gradient $\Delta p\mathrm{H} = -5$ at room temperature. The reorganization energies correspond to set (i) described before.

It follows from figure 4 that the system performs very well in a wide range of surface voltage gradients, from $\Delta V \sim 230$ up to $\Delta V \sim 350$ meV, translocating more than 40 protons and 20 electrons (in 100 μs). These numbers are almost the same for both sets of parameters (see figures 4(*a*) and (*b*)). The quantum yield QY monotonically goes down, from QY ~ 2 at $\Delta V \sim 200$ meV to QY ~ 1.5 at $\Delta V \sim 350$ meV, no matter which set is chosen. The power-conversion efficiency η also decreases with increasing ΔV. However, η is higher for the second set of parameters. For example, at $\Delta V = 260$ meV, the efficiency is about 31% for the first set, and $\eta \sim 47\%$ for the second set (with QY $= 1.9$) where both electron and proton electrochemical gradients are higher. This trend is consistent with equation (15) derived for the passenger scenario.

5. Conclusions and outlook

We have theoretically examined a model of the proton-motive force generation by the Q-cycle mechanism mimicking the operation of the *bf* complex in the thylakoid membranes of plants and cyanobacteria. We concentrate on a simulation of the regime of ferredoxin-dependent cyclic electron flow, where the *bf* complex translocates up to two protons (a quantum yield QY $= 2$) across the membrane per one electron transferred from the electron source (ferredoxin pool) to the electron drain (pool of plastocyanin molecules). This model includes two electron and two proton sites on the shuttle Q (an analog of a plastoquinone molecule), diffusing inside the membrane, as well as two electron sites, A and B, connecting the electron sites on the shuttle to the source and drain reservoirs. The recycling of an electron by the cytochrome *b*, which forms the basis of the Q-cycle, can be described by adding two electron sites L and H corresponding to the hemes b_L and b_H of the *bf* complex.

We have derived and numerically solved a set of master equations for the populations of the electron- and proton-binding sites together with a Langevin equation for the position of the shuttle. Within a reasonable scenario and in the presence of the surface potential, we have determined the conditions which are necessary for the efficient translocation of protons across the membrane. We have found that the system is able to transfer, on average, about 1.8 protons per one electron (QY $= 1.8$) with a thermodynamic efficiency of the order of 32% against the transmembrane proton gradient $\mu_P - \mu_N = 150$ meV at the source–drain difference of electron potentials $\mu_S - \mu_D = 850$ meV. These values of the electron and proton gradients are closely related to experimental values for the *bf* complex. No conformational gating is necessary for the bifurcation of the electron transfer reaction at the P-side catalytic center, where one electron goes to the drain and another electron returns to the L–H chain, to be loaded on the shuttle again. We have studied the performance of the model as a function of the proton electrochemical gradient and the surface potential. It is shown that the system demonstrates even better results, with a quantum yield of the order of 1.9 and an efficiency of the order of 47%, when both the source–drain difference and the proton gradient are higher.

The effects of the surface potential gradient, ΔV, and the proton gradient, $\mu_P - \mu_N$, on the electron and proton transfer can be tested in experiments. We note that the slowing of electron and proton flow through the system with increasing proton gradient can be important for turning on mechanisms of nonphotochemical quenching protecting the complex against the excessive light. An interaction of electron and proton circuits with the protein environment should also has a pronounced effect on the operation of the Q-cycle.

The present model can be generalized to the case of the LEF where all electrons participating in the Q-cycle are delivered to the system by the pool of external quinol molecules QH_2. We could also consider an internal pool of Q/QH_2 molecules instead of a single molecular shuttle analyzed above. Swinging of the ISP hinge at the P-side of the membrane can be included into consideration as well. This motion should be helpful for suppressing short-circuiting at the P-center. In order to explain an operation of the Q-cycle in the natural *bf* and bc_1 complexes having dimeric structures, it is necessary to build a model, which includes twice as many electron- and proton-binding sites as the present model.

Acknowledgments

FN acknowledges partial support from the Laboratory of Physical Sciences, National Security Agency, Army Research

Office, National Science Foundation grant no 0726909, JSPS-RFBR contract no 09-02-92114, Grant-in-Aid for Scientific Research (S), MEXT Kakenhi on Quantum Cybernetics and JSPS via its FIRST program.

Appendix. Master equations for electron-driven proton transfer across a membrane

Here we briefly outline a set of master equations describing the process of electron-driven proton translocation across a membrane. A detailed derivation of these equations can be found in the supporting information section available at stacks.iop.org/PhysBio/9/016011/mmedia. As we mentioned before, the total system is characterized by the average populations of the A and B sites, $\langle n_{\rm A}\rangle$, $\langle n_{\rm B}\rangle$, as well as by four states of the LH-subsystem with electron distributions $\langle R_M\rangle$ ($M = 1,\ldots,4$) and 16 states of the Q-subsystem (electrons and protons on the shuttle) with distributions $\langle \rho_\mu\rangle$ ($\mu = 1,\ldots,16$).

The time evolution of the LH-system is governed by the equation

$$\langle \dot R_M\rangle = -\sum_N \gamma^{\rm LH}_{NM}\,\langle R_M\rangle + \sum_N \gamma^{\rm LH}_{MN}\,\langle R_N\rangle, \tag{A.1}$$

with the following relaxation matrix:

$$\gamma^{\rm LH}_{MN} = \gamma^{\rm tun}_{MN} + \gamma^{\rm LQ}_{MN} + \gamma^{\rm HQ}_{MN}. \tag{A.2}$$

Here the rate

$$\gamma^{\rm tun}_{MN} = |\Delta_{\rm LH}|^2\sqrt{\frac{\pi}{\lambda_{\rm LH}T}}\left\{\left|\left\langle M\left|a^\dagger_{\rm L}a_{\rm H}\right|N\right\rangle\right|^2 + \left|\left\langle N\left|a^\dagger_{\rm L}a_{\rm H}\right|M\right\rangle\right|^2\right\} \times \exp\left[-\frac{(\Omega_{MN}+\lambda_{\rm LH})^2}{4\lambda_{\rm LH}T}\right] \tag{A.3}$$

describes the L-to-H electron transitions. Hereafter, $a^\dagger_\alpha$ and a_α refer to the creation and annihilation operators, respectively, for an electron on the site α. For protons on the site β, the creation and annihilation operators are denoted by $\mathrm{A}^\dagger_\beta$ and A_β, respectively. The rate $\gamma^{\rm LQ}_{MN}$ (and a similar rate $\gamma^{\rm HQ}_{MN}$) is related to the electron transfer between the L (or H) sites and the sites $1_{\rm e}$, $2_{\rm e}$ on the shuttle,

$$\gamma^{\rm LQ}_{MN} = |\Delta_{\rm LQ}|^2\sqrt{\frac{\pi}{\lambda_{\rm LQ}T}}\sum_{\mu\nu}|\langle\mu|a_1+a_2|\nu\rangle|^2 \times\left\{|\langle M|a_{\rm L}|N\rangle|^2\exp\left[-\frac{(\Omega_{MN}-\omega_{\mu\nu}+\lambda_{\rm LQ})^2}{4\lambda_{\rm LH}T}\right]\langle\rho_\mu\rangle + |\langle N|a_{\rm L}|M\rangle|^2\exp\left[-\frac{(\Omega_{MN}+\omega_{\mu\nu}+\lambda_{\rm LQ})^2}{4\lambda_{\rm LH}T}\right]\langle\rho_\nu\rangle\right\}, \tag{A.4}$$

where a_1 and a_2 are operators of the electron-binding sites on the shuttle, $\Omega_{MN} = E_M - E_N$ are frequencies of the LH-system ($\hbar = 1$, $k_B = 1$) and $\omega_{\mu\nu}$ is the frequency spectrum of the coupled electron–proton states on the shuttle Q.

For the distributions $\langle\rho_\mu\rangle$ of the 16 states of the Q-system, we derive the following equation:

$$\langle\dot\rho_\mu\rangle = -\sum_\nu \gamma^{\rm Q}_{\nu\mu}\,\langle\rho_\mu\rangle + \sum_\nu \gamma^{\rm Q}_{\mu\nu}\,\langle\rho_\nu\rangle, \tag{A.5}$$

where

$$\gamma^{\rm Q}_{\mu\nu} = \gamma^{\rm AQ}_{\mu\nu} + \gamma^{\rm BQ}_{\mu\nu} + \gamma^{\rm LQ}_{\mu\nu} + \gamma^{\rm HQ}_{\mu\nu} + \gamma^{\rm NQ}_{\mu\nu} + \gamma^{\rm PQ}_{\mu\nu}. \tag{A.6}$$

The components of this relaxation matrix can be written as

$$\gamma^{\rm AQ}_{\mu\nu} = |\Delta_{\rm AQ}|^2\sqrt{\frac{\pi}{\lambda_{\rm AQ}T}} \times\left\{|\langle\mu|a_1+a_2|\nu\rangle|^2\exp\left[-\frac{(\omega_{\mu\nu}+\varepsilon_{\rm A}+\lambda_{\rm AQ})^2}{4\lambda_{\rm AQ}T}\right]\langle 1-n_{\rm A}\rangle + |\langle\nu|a_1+a_2|\mu\rangle|^2\exp\left[-\frac{(\omega_{\mu\nu}-\varepsilon_{\rm A}+\lambda_{\rm AQ})^2}{4\lambda_{\rm AQ}T}\right]\langle n_{\rm A}\rangle\right\}, \tag{A.7}$$

with a similar matrix $\gamma^{\rm BQ}_{\mu\nu}$, and

$$\gamma^{\rm LQ}_{\mu\nu} = |\Delta_{\rm LQ}|^2\sqrt{\frac{\pi}{\lambda_{\rm LQ}T}}\sum_{MN}|\langle M|a_{\rm L}|N\rangle|^2 \times\left\{|\langle\nu|a_1+a_2|\mu\rangle|^2\langle R_N\rangle\exp\left[-\frac{(\omega_{\mu\nu}+\Omega_{MN}+\lambda_{\rm LQ})^2}{4\lambda_{\rm LQ}T}\right] + |\langle\mu|a_1+a_2|\nu\rangle|^2\langle R_M\rangle\exp\left[-\frac{(\omega_{\mu\nu}-\Omega_{MN}+\lambda_{\rm AQ})^2}{4\lambda_{\rm LQ}T}\right]\right\}, \tag{A.8}$$

with a matrix $\gamma^{\rm HQ}_{\mu\nu}$, which is similar to $\gamma^{\rm LQ}_{\mu\nu}$. The proton transitions to and from the shuttle are described by the rate

$$\gamma^{NQ}_{\mu\nu} = \Gamma_N|\langle\mu|{\rm A}_1+{\rm A}_2|\nu\rangle|^2[1-F_N(\omega_{\nu\mu})] + \Gamma_N|\langle\nu|{\rm A}_1+{\rm A}_2|\mu\rangle|^2F_N(\omega_{\mu\nu}), \tag{A.9}$$

and by a similar rate $\gamma^{\rm PQ}_{\mu\nu}$. Here

$$F_\sigma(E) = \left[\exp\left(\frac{E-\mu_\sigma}{T}\right)+1\right]^{-1} \tag{A.10}$$

is the Fermi distribution of the protons in the σ-reservoir ($\sigma = {\rm N}, {\rm P}$).

The average population of the A-site is governed by the equation

$$\langle\dot{\rm n}_A\rangle = \gamma_{\rm S}\left[f_{\rm S}(\varepsilon_{\rm A}) - \langle n_{\rm A}\rangle\right] + |\Delta_{\rm AQ}|^2\sqrt{\frac{\pi}{\lambda_{\rm AQ}T}}\sum_{\mu\nu}|\langle\mu|a_1+a_2|\nu\rangle|^2 \times\left\{\langle 1-n_{\rm A}\rangle\exp\left[-\frac{(\omega_{\mu\nu}+\varepsilon_{\rm A}+\lambda_{\rm AQ})^2}{4\lambda_{\rm AQ}T}\right]\langle\rho_\nu\rangle - \langle n_{\rm A}\rangle\exp\left[-\frac{(\omega_{\mu\nu}+\varepsilon_{\rm A}-\lambda_{\rm AQ})^2}{4\lambda_{\rm AQ}T}\right]\langle\rho_\mu\rangle\right\}, \tag{A.11}$$

where a coefficient $\gamma_{\rm S}$ (or $\gamma_{\rm D}$) describes the electron transitions from the A (or B) site to the source S (drain D) electron reservoir characterized by a Fermi distribution with the electrochemical potential $\mu_{\rm S}$ or $\mu_{\rm D}$ ($\alpha = {\rm S}, {\rm D}$),

$$f_\alpha(\varepsilon) = \left[\exp\left(\frac{\varepsilon-\mu_\alpha}{T}\right)+1\right]^{-1}. \tag{A.12}$$

A similar equation takes place for the population $\langle n_{\rm B}\rangle$.

We solve the rate equations (A.1), (A.5) and (A.11) for both the distributions $\langle R_M\rangle$, $\langle\rho_\mu\rangle$ and for the populations $\langle n_{\rm A}\rangle$ and $\langle n_{\rm B}\rangle$, together with an overdamped Langevin equation for the mechanical motion of the shuttle,

$$\zeta\,\dot x = -\frac{{\rm d}U_{\rm w}}{{\rm d}x} - \langle(n_1+n_2-N_1-N_2)^2\rangle\,\frac{{\rm d}U_{\rm ch}}{{\rm d}x} + \xi, \tag{A.13}$$

where ζ is the drag coefficient, ξ is a Gaussian fluctuation source with zero mean value, $\langle\xi\rangle = 0$, and with a correlator $\langle\xi(t)\xi(t')\rangle = 2\zeta T\delta(t-t')$. The potential $U_{\rm w}(x)$ confines the shuttle between the membrane walls, and the potential $U_{\rm ch}(x)$ prevents the charged molecule Q from crossing the lipid core of the membrane (for details, see [30]). We note that the tunneling amplitudes $\Delta_{\rm AQ}$, $\Delta_{\rm HQ}$ and the proton rate $\Gamma_{\rm N}$ depend on the distance between the shuttle (with a coordinate x) and the N-side catalytic center located at $x = -x_0$, whereas the tunneling amplitudes $\Delta_{\rm BQ}$, $\Delta_{\rm LQ}$ and the proton rate $\Gamma_{\rm P}$ depend on the distance between the shuttle and the P-side catalytic center located at $x = x_0$.

References

[1] LaVan D A and Cha J N 2006 Approaches for biological and biomimetic energy conversion *Proc. Natl Acad. Sci. USA* **103** 5251–5

[2] Kamat P V 2007 Meeting the clean energy demand: Nanostructure architectures for solar energy conversion *J. Phys. Chem. C* **111** 2834–60

[3] Nozik A J 2008 Multiple exciton generation in semiconductor quantum dots *Chem. Phys. Lett.* **457** 3–11

[4] Schaller R D and Klimov V I 2004 High efficiency carrier multiplication in PbSe nanocrystals: implications for solar energy conversion *Phys. Rev. Lett.* **92** 186601

[5] Kurisu G, Zhang H, Smith J L and Cramer W A 2003 Structure of the cytochrome b_6f complex of oxygenic photosynthesis: tuning the cavity *Science* **302** 1009–14

[6] Stroebel D, Choquet Y, Popot J-L and Picot D 2003 An atypical haem in the cytochrome b_6f complex *Nature* **426** 413–8

[7] Nicholls D G and Ferguson S J 2002 *Bioenergetics 3* (London: Academic)

[8] Mitchell P 1976 Possible molecular mechanisms of the protonmotive function of cytochrome systems *J. Theor. Biol.* **62** 327–67

[9] Osyczka A, Moser C C and Dutton P L 2005 Fixing the Q cycle *Trends Biochem. Sci.* **30** 176–82

[10] Crofts A R, Lhee S, Crofts S B, Cheng J and Rose S 2006 Proton pumping in the bc_1 complex: a new gating mechanism that prevents short circuits *Biochim. Biophys. Acta* **1757** 1019–34

[11] Richardson D and Sawers G 2002 PMF through the redox loop *Science* **295** 1842–43

[12] Osyczka A, Moser C C, Daldal F and Dutton P L 2004 Reversible redox energy coupling in electron transfer chains *Nature* **427** 607–12

[13] Cape J L, Bowman M K and Kramer D M 2006 Understanding the cytochrome *bc* complexes by what they don't do. The Q-cycle at 30 *Trends Plant Sci.* **11** 1360–85

[14] Mulkidjanian A Y 2010 Activated Q-cycle as a common mechanism for cytochrome bc_1 and cytochrome b_6f complexes *Biochim. Biophys. Acta* **1797** 1858–68

[15] Cramer W A, Hasan S S and Yamashita E 2011 The Q cycle of cytochrome *bc* complexes: a structure perspective *Biochim. Biophys. Acta* **1807** 788–802

[16] Joliot P, Joliot A and Johnson G 2006 Cyclic electron transfer around photosystem I *Photosystem I: The Light-Driven Plastocyanin: Ferredoxin Oxidoreductase* ed J H Golbeck (Berlin: Springer) pp 639–56

[17] Joliot P and Johnson G 2011 Regulation of cyclic and linear electron flow in higher plants *Proc. Natl Acad. Sci. USA* **108** 13317–22

[18] Shikanai T 2007 Cyclic electron transport around photosystem I: genetic approaches *Annu. Rev. Plant Biol.* **58** 199–217

[19] Iwai M, Takizawa K, Tokutsu R, Okamuro A, Takahashi Y and Minagawa J 2010 Isolation of the elusive supercomplex that drives cyclic electron flow in photosynthesis *Nature* **464** 1210–14

[20] Wikström M K 1972 Oxidoreduction of cytochrome *b* in the presence of antimycin *Biochim. Biophys. Acta* **283** 403–20

[21] Joliot P and Joliot A 2005 Quantification of cyclic and linear flows in plants *Proc. Natl Acad. Sci. USA* **102** 4913–8

[22] Munekage Y, Hashimoto M, Miake C, Tomizawa K I, Endo T, Tasaka M and Shikanai T 2004 Cyclic electron flow around photosystem I is essential for photosynthesis *Nature* **429** 579–82

[23] Cramer W A, Zhang H, Yan J, Kurisu G and Smith J L 2006 Transmembrane traffic in the cytochrome b_6f complex *Annu. Rev. Biochem.* **75** 769–90

[24] Heinmann S, Ponamarev M V and Cramer W A 2000 Movement of the rieske iron–sulfur protein in the *p*-side bulk aqueous phase: effect of lumenal viscosity on redox reactions of the cytochrome b_6f complex *Biochemistry* **39** 2692–99

[25] Zhang Z, Huang L, Shulmeister V M, Chi Y I, Kim K K, Hung L-W, Crofts A R, Berry E A and Kim S-H 1998 Electron transfer by domain movement in cytochrome bc_1 *Nature* **392** 677–84

[26] Crofts A R 2004 The Cytochrome bc_1 complex: function in the context of structure *Annu. Rev. Physiol.* **66** 689–733

[27] Yan J and Cramer W A 2003 Functional insensitivity of the cytochrome b_6f complex to structure changes in the hinge region of the rieske iron–sulfur protein *J. Biol. Chem.* **278** 20925–33

[28] Banilius D, Yamashita E, Zhang H, Hasan S S and Cramer W A 2008 Structure–function of the cytochrome b_6f complex *Photochem. Photobiol.* **84** 1349–58

[29] Marchal D, Boireau W, Laval J M, Moiroux J and Bourdillon C 1998 Electrochemical measurement of lateral diffusion coefficients of ubiquinones and plastoquinones of various isoprenoid chain lengths incorporated in model bilayers *Biophys. J.* **74** 1937–48

[30] Smirnov A Y, Savel'ev S E and Nori F 2009 Diffusion-controlled generation of a proton-motive force across a biomembrane *Phys. Rev.* E **80** 011916

[31] Smirnov A Y, Mourokh L G and Nori F 2011 Electrostatic models of electron-driven proton transfer across a lipid membrane *J. Phys.: Condens. Matter* **23** 234101

[32] Ghosh P K, Smirnov A Y and Nori F 2009 Modeling light-driven proton pumps in artificial photosynthetic reaction centers *J. Chem. Phys.* **131** 035102

[33] Smirnov A Y, Mourokh L G, Ghosh P K and Nori F 2009 High-efficiency energy conversion in a molecular triad connected to conducting leads *J. Phys. Chem. C* **113** 21218–24

[34] Cherepanov D A, Krishtalik L I and Mulkidjanian A Y 2001 Photosynthetic electron transfer controlled by protein relaxation: analysis by langevin stochastic approach *Biophys. J.* **80** 1033–49

[35] Hangarter R P, Jones R W, Ort D R and Whitmarsh J 1987 Stoichiometries and energetics of proton translocation coupled to electron transport in chloroplasts *Biochim. Biophys. Acta* **890** 106–15

[36] Berry S and Rumberg B 1999 Proton to electron stoichiometry in electron transport of spinach thylakoids *Biochim. Biophys. Acta* **1410** 248–61

[37] Okamura M Y, Paddock M L, Graige M S and Feher G 2000 Proton and electron transfer in bacterial reaction centers *Biochim. Biophys. Acta* **1458** 148–63